Ferroelectric Switchable Topological Magnon Hall Effect in Type-I Multiferroics

Quanchao Du, † Jinlian Lu, ‡ Xueqing Wan, † Zhenlong Zhang, *,† and Zhijun Jiang *,†

†Ministry of Education Key Laboratory for Nonequilibrium Synthesis and Modulation of Condensed Matter, Shaanxi Province Key Laboratory of Advanced Functional Materials and Mesoscopic Physics, School of Physics, Xi'an Jiaotong University, Xi'an 710049, China †Department of Physics, Yancheng Institute of Technology, Yancheng, Jiangsu 224051, China

E-mail: zhangzl@stu.xjtu.edu.cn; zjjiang@xjtu.edu.cn

Abstract

Electric control of magnetism at room temperature is crucial for developing next-generation,

low-power spintronic devices. However, the intrinsic incompatibility between ferroelectricity

and magnetism in crystal symmetry, along with the absence of strong magnetoelectric

coupling mechanisms, continues to pose major challenges. In this work, we propose a

general theoretical framework for magnon manipulation based on ferroelectric polarization

switching in two-dimensional multiferroics. Taking monolayer multiferroics Ti₂F₃ as an

example, our calculations demonstrate that ferroelectric switching can significantly modulate

spin exchanges, thereby enabling nonvolatile and reversible electric control of the magnons.

More importantly, the ferroelectric polarization reversal leads to a sign change in the Berry

curvature, ensuring effective control over the valley Hall and nonlinear Hall response of

magnons. This study provides a new way for realizing low-power and electrically controllable

magnonic devices.

Keywords: Magnetoelectric coupling, Multiferroics, Magnons, Magnon Hall current

2

Introduction. Electric control of magnetism offers a most promising pathway for next-generation and high-performance spintronic devices, such as nonvolatile memory and low-power sensors ^{1–3}. One promising approach is through the magnetoelectric (ME) coupling effect in multiferroics, where ferroelectric and magnetic orders coexist within a single phase ^{4–9}. Crucially, realizing the room-temperature multiferroics with strong ME coupling remains the significant challenges ¹⁰. In the so-called type-II multiferroics (e.g., TbMnO₃), although the intrinsic ME coupling is strong, the electric polarization induced by non-centrosymmetric spin order is typically quite small ^{7,11,12}. Type-I multiferroics generally exhibit strong ferroelectricity and magnetism, but since these two orders originate from different mechanisms, the resulting ME coupling is usually weak ^{4,13,14}. Therefore, from both fundamental and application perspectives, discovering new mechanisms that enable efficient electrical control of magnetism is of great scientific importance and practical relevance.

In addition to the spin orders, electric-field manipulation of spin excited states has recently emerged as a promising way. Particularly in magnetic insulators, magnons act as their charge-neutral quasiparticles of collective spin excitations, carrying spin angular momentum while effectively avoiding the Joule heating typically associated with charge transport ^{15–17}. Therefore, achieving electric-field control of magnons holds significant potential for magnetic insulators. Recent studies have shown that an applied electric field can modulate the spin exchanges via the strong spin-layer coupling. This mechanism enables nonvolatile control of magnons, including their topological and transport properties ^{18–21}. However, from the perspective of control efficiency, leveraging ferroelectric switching in multiferroics to manipulate the magnons represents a more effective approach, yet it remains largely unexplored.

In this work, we demonstrate that the ferroelectric-switching magnon Hall effect mechanism in Type-I multiferroics ${\rm Ti}_2{\rm F}_3$ 22,23 . Our results show that, the ferroelectricity in ${\rm Ti}_2{\rm F}_3$ originate from the lattice distortion, which leads to the weak intrinsic ME coupling. However, ferroelectric polarization breaks the sublattice symmetry of the honeycomb ferromagnetic lattice, which ensure that ferroelectric switching is accompanied by a reversal of their magnon valley index. Consequently, ferroelectricity opens Dirac points for magnons at the valley points and induces nonzero Berry curvature. Since the Berry curvature determines the

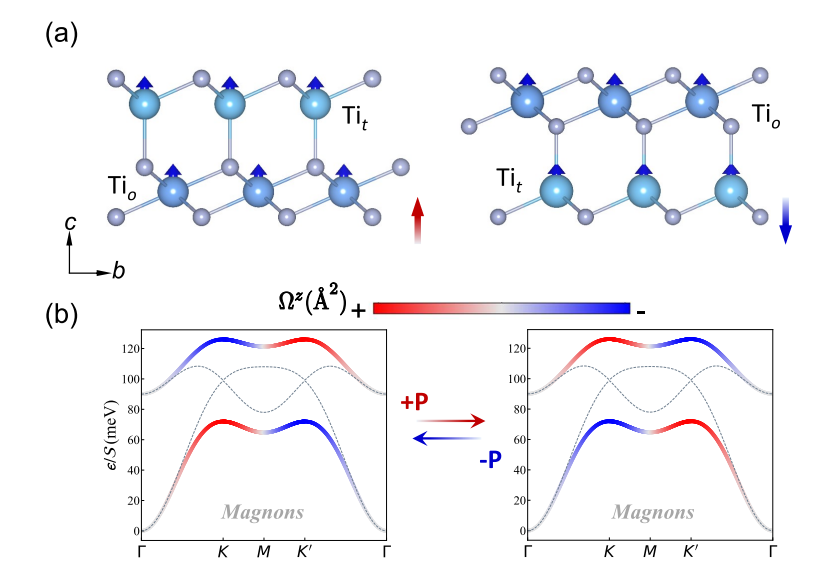


Figure 1: (a) The side view of the monolayer Ti_2F_3 showing different out-of-plane polarization P configuration, labeled as FE-up and FE-dn, respectively. (b) Magnon bands of Ti_2F_3 weighted by the Berry curvature Ω^z for FE-up (left) and FE-dn (right) states. Switching the polarization from +P to -P reverses the sign of Ω^z .

magnon valley Hall response, ferroelectric switching also reverses the corresponding valley transport. Importantly, although the weak spin-orbit coupling Ti₂F₃ leads to a negligible linear thermal Hall response, the nonlinear Hall effect arising from inversion symmetry breaking is highly robust and can likewise be efficiently controlled through ferroelectric switching.

Magnetic properties of Ti_2F_3 . Monolayer Ti_2F_3 adopt the P3m1 polar space group, with its structure illustrated in Figure 1(a). The ferroelectricity in monolayer Ti_2F_3 originates from the charge transfer between the Ti magnetic ions and F anions. This charge redistribution drives the system into an insulating state and simultaneously induces lattice distortions in the Ti-F sub-layer, as shown in Figure 2(c)-(d). Consequently, in ferroelectric-up configuration (FE-up), the upper Ti-F sub-layer adopts a TiF_4 tetrahedral geometry (Ti_t) , whereas the down Ti-F sub-layer exhibits a TiF_6 octahedral coordination environment $(Ti_o)^{22,23}$. In the ferroelectric-down (FE-dn) configuration, this arrangement is reversed. The stability of the ferroelectric monolayer Ti_2F_3 is confirmed by the first principles phonons calculations, as shown in Figure S1 ²⁴. The energy barrier between the FE-up and Fe-dn state is also calculated by the Nudged-Elastic-Band (NEB) theory ²⁵ (see Figure 2(c)). Based on their

relative positions, Ti magnetic ions in the unit cell can be distinguished into two sublattices, Ti_t and Ti_o , which are convertible upon ferroelectric switching.

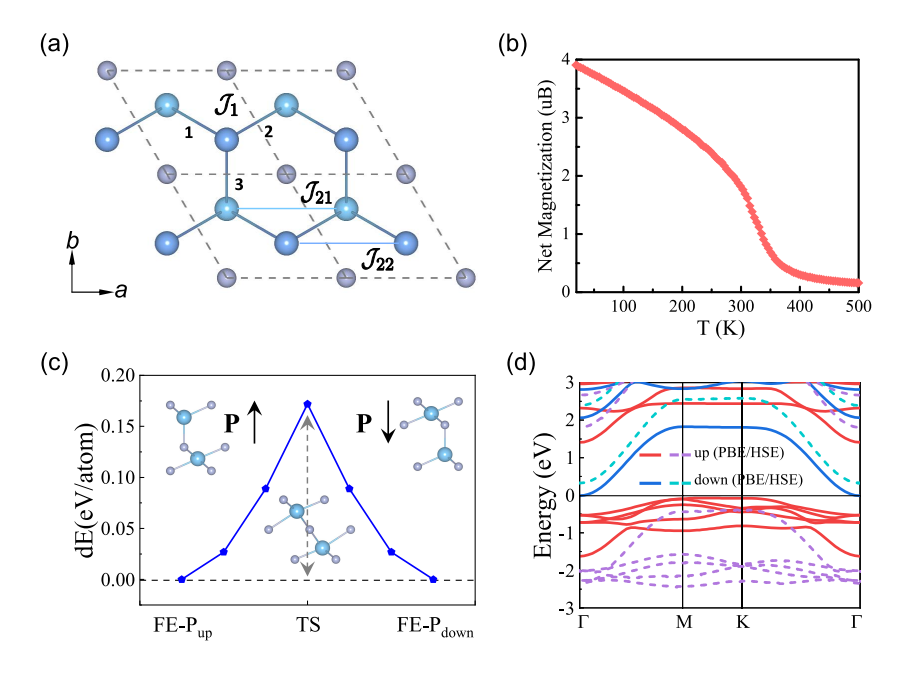


Figure 2: (a) Top view of the monolayer Ti_2F_3 structure with labeling the spin exchanges. Here, light and dark blue ions refer to the Ti_t and Ti_o , respectively. (b) Temperature dependence of the net magnetization Ti_2F_3 obtained from MC simulations. (c) The FE switching barrier of monolayer Ti_2F_3 . (d) The band structure of the monolayer Ti_2F_3 .

Evidently, the top view of the Ti magnetic ions in monolayer Ti₂F₃ forms a ferromagnetic honeycomb lattice, as shown in Figure 2(a). In this context, nearest-neighbor (NN) intralayer spin exchange between Ti ions corresponds to NN spin exchange of the honeycomb lattice, while NN spin exchange between Ti magnetic ions corresponds to second-nearest-neighbor (2NN) spin exchange. DFT calculations reveal that all NN spin exchanges between the Ti magnetic ions exhibit ferromagnetic character. Since the weak spin-orbit coupling, the spin Hamiltonian for the Ti₂F₃ monolayer can be well described by the Heisenberg model, given by

$$\hat{\mathcal{H}} = \mathcal{J}_1 \sum_{\langle i,j \rangle} \mathcal{S}_i \cdot \mathcal{S}_j + \mathcal{J}_{21} \sum_{\langle i,j \rangle} \mathcal{S}_i \cdot \mathcal{S}_j + \mathcal{J}_{22} \sum_{\langle i,j \rangle} \mathcal{S}_i \cdot \mathcal{S}_j, \tag{1}$$

where \mathcal{J}_1 is the NN interlayer spin exchange between Ti_o and Ti_t , $\mathcal{J}_{21(22)}$ denotes NN intralayer spin exchange between Ti_o - Ti_o (Ti_t - Ti_t) ions. Based on the LKAG method $^{26-28}$,

the \mathcal{J}_1 , \mathcal{J}_{21} , and \mathcal{J}_{22} is obtained, with values of that -30, -10 and -5 meV, respectively. The Monte Carlo (MC) simulations ²⁴, as presented in Figure 2(b), indicate that ferromagnetic transition temperature (T_c) of approximately 340 K, which is above room temperature.

Within the ferromagnetic order, the linear spin wave (LSW) model in Eq.(1) can be solved by employing the Holstein-Primakoff (HP)²⁹, $S_{i,\alpha}^z = S - \hat{a}_{i,\alpha}^{\dagger} \hat{a}_{i,\alpha}$, $S_i^+ \approx \sqrt{2S} \hat{a}_{i,\alpha}$, and $S_i^- \approx \sqrt{2S} \hat{a}_{i,\alpha}^{\dagger}$, with $\hat{a}_{i,\alpha}^{\dagger} (\hat{a}_{i,\alpha}^{\dagger})$ creating a magnon at sublattice in the honeycomb unit cell. After the Fourier transformation, the Hamiltonian can be expressed in momentum space using the basis $\psi_k^{\dagger} \equiv (\hat{a}_k^{\dagger}, \hat{b}_k^{\dagger})$ as $\hat{\mathcal{H}} = \sum_k \psi_k^{\dagger} \hat{\mathcal{H}}_k \psi_k$. Neglecting the zero-point energy, the $\hat{\mathcal{H}}_k$ reads as,

$$\frac{\hat{\mathcal{H}}_k}{S} = -3\mathcal{J}_1 + \begin{pmatrix} \mathcal{J}_{21}f_k & \mathcal{J}_1\gamma_k \\ \mathcal{J}_1\gamma_k^{\dagger} & \mathcal{J}_{22}f_k \end{pmatrix},\tag{2}$$

where $\gamma_k = \sum_{\delta} e^{-i\mathbf{k}\cdot\mathbf{\delta}_i}$ and $f_k = \sum_{i \in odd} 2\cos(\mathbf{k}\cdot\boldsymbol{\mu}_i) - 6$ with $\boldsymbol{\delta}_i$ and $\boldsymbol{\mu}_i$ being NN and 2NN linking vectors of honeycomb lattice as shown in Figure 2(a).

We further parameterize Eq. (2) as $h_0 = \frac{1}{2}(\mathcal{J}_{21} + \mathcal{J}_{22})f_k$, $h_x = \mathcal{J}_1 \text{Re}\gamma_k$, $h_y = \mathcal{J}_1 \text{Im}\gamma_k$ and $h_z = \frac{1}{2}(\mathcal{J}_{21} - \mathcal{J}_{22})f_k$. Eq. (2) can thus be expressed in terms of the Pauli matrices $\boldsymbol{\sigma} = (\sigma_x, \sigma_y, \sigma_z)$ as

$$\frac{\hat{\mathcal{H}}_k}{S} = h_0 I + \boldsymbol{h}(\boldsymbol{k}) \cdot \boldsymbol{\sigma},\tag{3}$$

where $\boldsymbol{h}(\boldsymbol{k}) = (h_x, h_y, h_z) = |h| (\sin\theta\cos\phi, \sin\theta\sin\phi, \cos\theta)$. As a result, the corresponding eigenvalues and eigenvectors are given as

$$\frac{\epsilon_{\pm}}{S} = h_0 \pm |\boldsymbol{h}(\boldsymbol{k})|, \quad \Psi_{\pm} = \begin{pmatrix} \sqrt{1 \pm \cos\theta} \\ \pm e^{-i\phi} \sqrt{1 \mp \cos\theta} \end{pmatrix}. \tag{4}$$

The presence of h_z explicitly breaks the sublattice symmetry of the honeycomb lattice, opening a gap in the magnon bands at the K-points. While time-reversal symmetry (\mathcal{T}) remains preserved ^{19,30}, the broken inversion symmetry (\mathcal{P}) leads to a nonzero Berry curvature. In 2D case, the Berry curvature only has z component ^{18,31}, which can be expressed in terms

of the h(k) vector

$$\Omega_{\pm}^{z}(\mathbf{k}) = -i\langle \nabla \Psi_{\pm} | \times | \nabla \Psi_{\pm} \rangle = \mp \frac{h_{z}}{2} \left(\nabla h_{x} \times \nabla h_{y} \right). \tag{5}$$

Therefore, the nonzero Berry curvature of magnons in monolayer Ti_2F_3 can be emerged in the ferroelectric states, in which nonzero of $\mathcal{J}_{21} - \mathcal{J}_{22}$ breaks the \mathcal{P} symmetry, leading to that $\Omega(\mathbf{k}) = -\Omega(-\mathbf{k})$. Notably, the sign of $\mathcal{J}_{21} - \mathcal{J}_{22}$ can be reversed through ferroelectric switching, enabling electrical control of the magnonic Berry curvature, as shown in the Figure 1(b) and Figure 3(b).

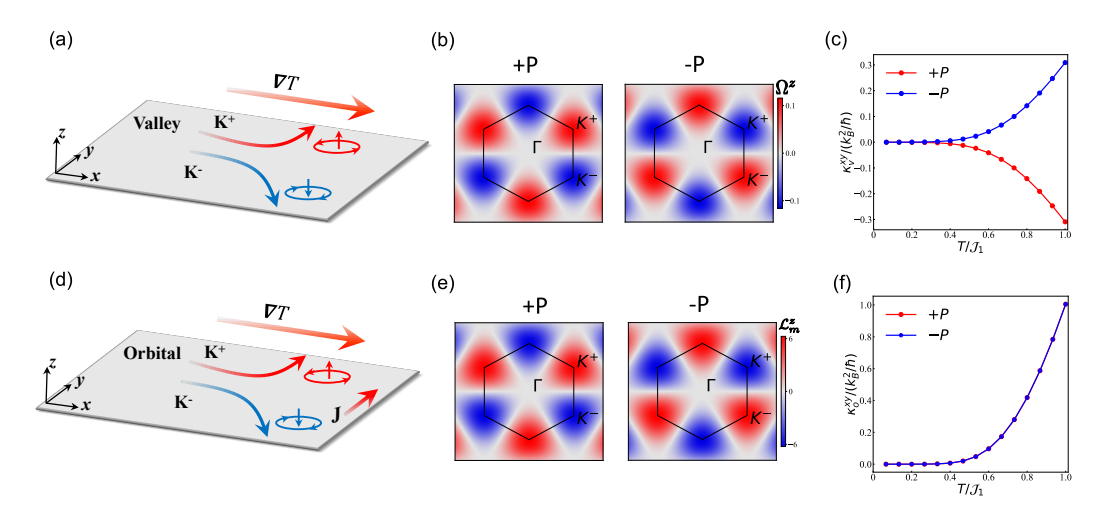


Figure 3: (a) The schematic of the magnon valley Hall effect. (b) The Berry curvature of the major magnon band with FE-up (left) and FE-dn (right) state. (c) The temperature dependence of the magnon valley Hall conductivity κ_v^{xy} . (d) The schematic of the magnon orbital Hall effect. (e) The orbital magnetic moment of the major magnon band with FE-up (left) and FE-dn (right) state. (f) The temperature dependence of the magnon orbital Hall conductivity κ_o^{xy} .

In addition to the Berry curvature, the emergence of h_z can induce orbital moments of magnons ^{18,32–34}. According to the previous work ^{31,35}, the orbital quantity of Bloch magnons can be expressed as

$$\mathcal{L}_{m,\pm}^{z}(\mathbf{k}) = -\frac{i}{2\hbar} \langle \nabla \Psi_{\pm} | \times (\hat{\mathcal{H}}_{k} - \epsilon_{k}) | \nabla \Psi_{\pm} \rangle. \tag{6}$$

As shown in Figure 3(e), orbital moments (\mathcal{L}_m^z) in the ferroelectric state mainly locate at the valley points, and their sign can be reversed through ferroelectric switching, similar to the behavior of the Berry curvature. Notably, the orbital moments exhibit the same

chirality for both the majority and minority magnon bands. Therefore, in monolayer Ti_2F_3 , the ferroelectricity breaks the \mathcal{P} symmetry of the honeycomb lattice, inducing finite Berry curvature and orbital magnetic moments in magnons, whose signs can be reversibly controlled through ferroelectric switching.

Magnon valley and orbital response. As shown in Figure 3, the Berry curvature of magnons with ferroelectric state is primarily concentrated at the K points, satisfying $\Omega(\mathbf{k}) = -\Omega(-\mathbf{k})$. In this case, the linear thermal Hall response under the temperature gradient remains zero due to the opposite contributions of magnon Berry curvature at K and K'-points. However, the opposite orbit pseudo-magnetic field at K and K'-points gives rise to the magnon valley current, similar to the gapped graphene 36,37 . To distinguish the difference between K and K'-points 38 , we define the magnon valley conductivity κ_{xy}^v as

$$\kappa_{xy}^{v} = \frac{k_B^2 T}{\hbar V} \sum_{n,k} c_2(\rho) \left[\Omega_{n,k}(\mathbf{K}) - \Omega_{n,k}(\mathbf{K}') \right], \tag{7}$$

where V is the volume, ε_{abc} is the Levi-Civita symbol with abc = xyz and $c_2(\rho) = \int_0^{\rho} [\log(1 + \rho^{-1})]^2 d\rho$ with ρ being Boltzmann distributions for bosons. Since the Berry curvature can be reversed by the ferroelectric switching, the sign of the magnon valley Hall conductivity κ_{xy}^v can be controlled by the ferroelectric polarization, as illustrated in Figure 3(c).

Next, we investigate the magnon orbital response in the ferroelectric Ti_2F_3 . The emergence of magnon orbital moments gives rise to the anomalous orbital associated transport phenomena ^{34,37}, in which the orbital Berry curvature, Ω_o^z is defined as

$$\Omega_o^z(\mathbf{k}) = \Omega^z(\mathbf{k}) \mathcal{L}_m^z(\mathbf{k}). \tag{8}$$

Obviously, the orbital Berry curvature is the product of the Berry curvature and the orbital moments of magnons 34,37 . As both the Berry curvature and orbital moments are odd with respect to \mathbf{k} , their product, orbital Berry curvature, is even, $\Omega_o^z(\mathbf{k}) = \Omega_o^z(-\mathbf{k})$. This feature enables the emergence of the magnon orbital Hall response, in contrast to the contribution from the Berry curvature alone. Analogous to the magnon Hall effect, the magnon orbital Hall conductivity can be determined by integrating the product of $c_2(p)$ and Ω_o^z over the

Brillouin zone, expressed as follows

$$\kappa_{xy}^o = \frac{k_B^2 T}{\hbar V} \sum_{n,k} c_2(\rho) \Omega_{n,o}^z(k). \tag{9}$$

As shown in Figure 3(f), we calculated the temperature-dependent magnon orbital Hall conductivity. Obviously, unlike the magnon valley Hall response, the orbital Hall conductivity remains unchanged across different ferroelectric states. This difference mainly arises from the fact that, although both the Berry curvature and the orbital moment can be reversed by ferroelectric polarization, their product—the orbital Berry curvature—remains invariant.

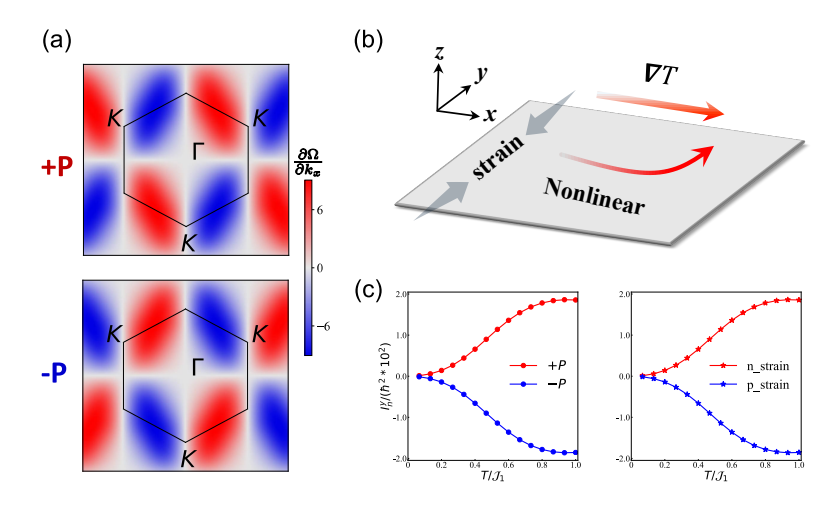


Figure 4: (a) The extended BCD of the major band with FE-up and FE-dn state. (b) The schematic illustration of the magnon nonlinear Hall effect. (c) The calculated temperature dependence of the magnon nonlinear Hall conductivity I_n^y . The left and right panels illustrate the reversal behavior induced by ferroelectric polarization switching and strain modulation, respectively.

Magnon nonlinear Hall response. Additionally, the \mathcal{P} breaking in magnons gives rise to the nonlinear Hall response. According to the previous works ^{39–41}, the magnon nonlinear Hall conductivity is given as

$$I_n^a \approx \frac{2\varepsilon_{abc}}{V\hbar^2 T} \sum_{n,k} c_1(\rho)\epsilon_{n,k}\partial_{k_b} \left[\Omega_{n,k}^c \epsilon_{n,k}\right],\tag{10}$$

where ε_{abc} is Levi-Civita symbol with abc = xyz and $c_1(\rho) = \int_0^{\rho} \log(1 + \rho^{-1}) d\rho$. In 2D case, c = z, indicating that the nonlinear transverse magnon current can emerge along y-

axis when applying ∇T along x-axis as shown in Figure 4(b). Obviously, I_n^y depends on the $\partial_{k_x}\Omega_{n,k}$, which is defined as the extended Berry curvature dipole (BCD) of magnons 40,41 . The extended BCD distribution of major band is shown Figure 4(a), which is even with respect to k and can be reversed by the ferroelectric switching. Notably, since the C_{3z} symmetry can transform k_m to k_μ and k_ν in k-space, allows $[\partial_{k_x}\Omega_{n,}]_{k_m} + [\partial_{k_x}\Omega_{n,}]_{k_\mu} + [\partial_{k_x}\Omega_{n,}]_{k_\nu} = 0$, suggesting the integral of Eq. (10) goes to zero. As shown in Figure 4(c) and Figure S3 24 , the nonzero sum of velocities can be generated by uniaxial strain, which breaks the C_{3z} symmetry and distributes the invariance among the three NN spin exchange interactions. When a little uniaxial strain perpendicular to the applied temperature gradient is introduced into the monolayer Ti_2F_3 , the pronounced nonlinear transverse magnon current can be emergent. Interestingly, in addition to ferroelectric switching, the direction of the applied uniaxial strain is also coupled to the sign of the nonlinear Hall response. As shown in Figure S3 24 and Figure 4(c), the nonlinear Hall response can be reversed by either the ferroelectric switching or the uniaxial strain.

Summary and discussion. In contrast to the linear magnon Hall response, which typically requires breaking the effective time-reversal symmetry via the Dzyaloshinskii-Moriya interaction (DMI) or bond-dependent spin exchanges ^{17,42–44}, the nonlinear Hall response in Ti₂F₃ arise from the lattice distortions. Importantly, both the ferroelectric and strain switching can reverse the sign of the nonlinear Hall conductivity. Therefore, although monolayer Ti₂F₃ exhibits weak spin-orbit coupling and a negligible linear Hall response, its robust nonlinear Hall effect, combined with tunability via external fields, endows it with significant potential for practical applications.

In summary, we reveal the mechanism by which ferroelectric switching modulates the topological magnon transport in monolayer multiferroics Ti₂F₃. Our results show that the ferroelectric distortion breaks the inversion symmetry of the hexagonal ferromagnetic lattice, enabling the Berry curvature and orbital magnetic moment of magnons to reverse with the ferroelectric polarization. Consequently, both the valley Hall transport and the nonlinear Hall effect are strongly coupled to the ferroelectric polarization. These findings provide important theoretical guidance for realizing high-performance and reconfigurable next-generation spintronic devices.

ASSOCIATED CONTENT

Supporting Information

In this Supporting Information, we provide: I. DFT calculations and Monte Carlo simulations

on monolayer Ti₂F₃; II. Topological geometry of magnons in monolayer Ti₂F₃.

Corresponding Authors

*E-mail: zhangzl@stu.xjtu.edu.cn (Z. Z.)

*E-mail: zjjiang@xjtu.edu.cn (Z. J.)

Notes

The authors declare no competing financial interest.

ACKNOWLEDGMENTS

The authors thank Prof. Jianli Wang and Prof. Jinyang Ni for helpful discussions. This work

is supported by the National Natural Science Foundation of China (Grant No. 12374092),

Natural Science Basic Research Program of Shaanxi (Program No. 2023-JC-YB-017), Shaanxi

Fundamental Science Research Project for Mathematics and Physics (Grant No. 22JSQ013),

"Young Talent Support Plan" of Xi'an Jiaotong University, and the Xiaomi Young Talents

Program.

References

(1) Ramesh, R.; Spaldin, N. A. Multiferroics: progress and prospects in thin films. Nat.

Mater. **2007**, 6, 21–29.

(2) Fiebig, M.; Lottermoser, T.; Meier, D.; Trassin, M. The evolution of multiferroics. Nat.

11

- Rev. Mater. 2016, 1, 1–14.
- (3) Schmid, H. Multi-ferroic magnetoelectrics. Ferroelectrics 1994, 162, 317–338.
- (4) Spaldin, N. A.; Cheong, S.-W.; Ramesh, R. Multiferroics: Past, present, and future. *Phys. Today* **2010**, *63*, 38–43.
- (5) Xu, C.; Chen, P.; Tan, H.; Yang, Y.; Xiang, H.; Bellaiche, L. Electric-field switching of magnetic topological charge in type-I multiferroics. *Phys. Rev. Lett.* **2020**, *125*, 037203.
- (6) Van Aken, B. B.; Palstra, T. T.; Filippetti, A.; Spaldin, N. A. The origin of ferroelectricity in magnetoelectric YMnO₃. *Nat. Mater.* **2004**, *3*, 164–170.
- (7) Kimura, T.; Goto, T.; Shintani, H.; Ishizaka, K.; Arima, T.-h.; Tokura, Y. Magnetic control of ferroelectric polarization. *Nature* **2003**, *426*, 55–58.
- (8) Song, Q.; Occhialini, C. A.; Ergeçen, E.; Ilyas, B.; Amoroso, D.; Barone, P.; Kapeghian, J.; Watanabe, K.; Taniguchi, T.; Botana, A. S.; Picozzi, S.; Gedik, N.; Comin, R. Evidence for a single-layer van der Waals multiferroic. *Nature* 2022, 602, 601–605.
- (9) Ponet, L.; Artyukhin, S.; Kain, T.; Wettstein, J.; Pimenov, A.; Shuvaev, A.; Wang, X.; Cheong, S.-W.; Mostovoy, M.; Pimenov, A. Topologically protected magnetoelectric switching in a multiferroic. *Nature* **2022**, *607*, 81–85.
- (10) Dong, S.; Xiang, H.; Dagotto, E. Magnetoelectricity in multiferroics: a theoretical perspective. *Nat. Sci. Rev.* **2019**, *6*, 629–641.
- (11) Malashevich, A.; Vanderbilt, D. First principles study of improper ferroelectricity in TbMnO₃. Phys. Rev. Lett. **2008**, 101, 037210.
- (12) Xiang, H. J.; Wei, S.-H.; Whangbo, M.-H.; Da Silva, J. L. F. Spin-orbit coupling and ion displacements in multiferroic TbMnO₃. *Phys. Rev. Lett.* **2008**, *101*, 037209.
- (13) Wang, J.; Neaton, J. B.; Zheng, H.; Nagarajan, V.; Ogale, S. B.; Liu, B.; Viehland, D.; Vaithyanathan, V.; Schlom, D. G.; Waghmare, U. V.; Spaldin, N. A.; Rabe, K. M.;

- Wuttig, M.; R., R. Epitaxial BiFeO₃ multiferroic thin film heterostructures. *Science* **2003**, *299*, 1719–1722.
- (14) Ni, J. Y.; Wang, P. S.; Lu, J. L.; Xiang, H. J. Realizing magnetoelectric coupling with hydrogen intercalation. *Phys. Rev. Lett.* **2019**, *122*, 117601.
- (15) Chumak, A. V.; Vasyuchka, V. I.; Serga, A. A.; Hillebrands, B. Magnon spintronics.

 Nat. Phys. 2015, 11, 453–461.
- (16) Lenk, B.; Ulrichs, H.; Garbs, F.; Münzenberg, M. The building blocks of magnonics. *Phys. Rep.* **2011**, *507*, 107–136.
- (17) Onose, Y.; Ideue, T.; Katsura, H.; Shiomi, Y.; Nagaosa, N.; Tokura, Y. Observation of the magnon Hall effect. *Science* **2010**, *329*, 297–299.
- (18) Ni, J.; Zhang, Z.; Lu, J.; Du, Q.; Jiang, Z.; Bellaiche, L. Nonvolatile magnonics in bilayer magnetic insulators. *Nano Lett.* **2025**, *25*, 1207–1213.
- (19) Wan, X.; Du, Q.; Lu, J.; Zhang, Z.; Ni, J.; Zhang, L.; Jiang, Z.; Bellaiche, L. Topological switching in bilayer magnons via electrical control. *Phys. Rev. B* **2025**, *112*, L100404.
- (20) Zhang, R.-W.; Cui, C.; Li, R.; Duan, J.; Li, L.; Yu, Z.-M.; Yao, Y. Predictable gate-field Control of spin in altermagnets with spin-layer coupling. *Phys. Rev. Lett.* **2024**, *133*, 056401.
- (21) Tian, J.; Li, J.; Liu, H.; Li, Y.; Liu, Z.; Li, L.; Li, J.; Liu, G.; Shi, J. Spin-layer coupling in an altermagnetic multilayer: A design principle for spintronics. *Phys. Rev. B* **2025**, 111, 035437.
- (22) Zhang, Y.; Chen, J.; Ye, H.; Wu, Z.; Zhang, G.; Gu, M.; Wang, J. Electric field tunable magnetic phase transition and magneto-optical effects in two-dimensional multiferroic Ti₂F₃ semiconductor. *Appl. Phys. Lett.* **2025**, *127*, 152904.
- (23) Sun, C.; Sun, Y.; Ye, H.; Zhu, Y.; Chen, L.; Li, H.; Zhang, G.; Wang, J. Anomalous valley Hall effect in two-dimensional multiferroic V₂N₂O semiconductor. *Appl. Phys. Lett.* **2025**, *127*, 142903.

- (24) I. DFT calculations and Monte Carlo simulations on monolayer Ti₂F₃; II. Topological geometry of magnons in monolayer Ti₂F₃
- (25) Sheppard, D.; Xiao, P.; Chemelewski, W.; Johnson, D. D.; Henkelman, G. A generalized solid-state nudged elastic band method. *J. Chem. Phys.* **2012**, *136*.
- (26) Liechtenstein, A. I.; Katsnelson, M.; Antropov, V.; Gubanov, V. Local spin density functional approach to the theory of exchange interactions in ferromagnetic metals and alloys. J. Magn. Magn. Mater. 1987, 67, 65–74.
- (27) Grotheer, O.; Ederer, C.; Fähnle, M. Fast ab initio methods for the calculation of adiabatic spin wave spectra in complex systems. *Phys. Rev. B* **2001**, *63*, 100401.
- (28) He, X.; Helbig, N.; Verstraete, M. J.; Bousquet, E. TB2J: A python package for computing magnetic interaction parameters. *Comput. Phys. Commun.* **2021**, *264*, 107938.
- (29) Holstein, T.; Primakoff, H. Field dependence of the intrinsic domain magnetization of a ferromagnet. *Phys. Rev.* **1940**, *58*, 1098.
- (30) Mook, A.; Plekhanov, K.; Klinovaja, J.; Loss, D. Interaction-stabilized topological magnon insulator in ferromagnets. *Phys. Rev. X* **2021**, *11*, 021061.
- (31) Xiao, D.; Chang, M.-C.; Niu, Q. Berry phase effects on electronic properties. *Rev. Mod. Phys.* **2010**, *82*, 1959–2007.
- (32) Neumann, R. R.; Mook, A.; Henk, J.; Mertig, I. Orbital magnetic moment of magnons. *Phys. Rev. Lett.* **2020**, *125*, 117209.
- (33) Fishman, R. S.; Gardner, J. S.; Okamoto, S. Orbital angular momentum of magnons in collinear magnets. *Phys. Rev. Lett.* **2022**, *129*, 167202.
- (34) Go, G.; An, D.; Lee, H.-W.; Kim, S. K. Magnon orbital Nernst effect in honeycomb antiferromagnets without spin-orbit coupling. *Nano Lett.* **2024**, *24*, 5968–5974.

- (35) Chang, M.-C.; Niu, Q. Berry phase, hyperorbits, and the Hofstadter spectrum: Semiclassical dynamics in magnetic Bloch bands. *Phys. Rev. B* **1996**, *53*, 7010.
- (36) Xiao, D.; Yao, W.; Niu, Q. Valley-contrasting physics in graphene: magnetic moment and topological transport. *Phys. Rev. Lett.* **2007**, *99*, 236809.
- (37) Bhowal, S.; Vignale, G. Orbital Hall effect as an alternative to valley Hall effect in gapped graphene. *Phys. Rev. B* **2021**, *103*, 195309.
- (38) Zhai, X.; Blanter, Y. M. Topological valley transport of gapped Dirac magnons in bilayer ferromagnetic insulators. *Phys. Rev. B* **2020**, *102*, 075407.
- (39) Ni, J.; Jin, Y.; Du, Q.; Chang, G. Magnon nonlinear Hall effect in two-dimensional antiferromagnetic insulators. *Phys. Rev. B* **2025**, *112*, 054424.
- (40) Mukherjee, R.; Verma, S.; Kundu, A. Nonlinear magnon transport in bilayer van der Waals antiferromagnets. *Phys. Rev. B* **2023**, *107*, 245426.
- (41) Kondo, H.; Akagi, Y. Nonlinear magnon spin Nernst effect in antiferromagnets and strain-tunable pure spin current. *Phys. Rev. Res.* **2022**, *4*, 013186.
- (42) Katsura, H.; Nagaosa, N.; Lee, P. A. Theory of the thermal Hall effect in quantum magnets. *Phys. Rev. Lett.* **2010**, *104*, 066403.
- (43) Zhang, X. T.; Gao, Y. H.; Chen, G. Thermal Hall effects in quantum magnets. *Phys. Rep.* **2024**, *1070*, 1–59.
- (44) Owerre, S. A first theoretical realization of honeycomb topological magnon insulator.

 J. Phys. Condens. Matter 2016, 28, 386001.